minerals

Article

Whole-Rock Geochemistry and Mica Compositions in Lijiagou Pegmatite Spodumene Deposit, Western Sichuan, China

Xiaojie Chen [1], Cuihua Chen [1,*], Xiang Lai [1], Yulong Yang [1], Ying Gu [1] and Yunhua Cai [2]

[1] College of Earth Science, Chengdu University of Technology, Chengdu 610059, China
[2] Geochemistry Exploration Team, The Sichuan Bureau of Geology and Mineral Resources, Deyang 618000, China
* Correspondence: chencuihua@cdut.edu.cn

Abstract: The Lijiagou pegmatite spodumene deposit, located in the middle of the Songpan–Garze Fold Belt and southeast of the Ke'eryin ore field, is a newly discovered super-large deposit. In order to reveal the metallogenic tectonic environment and evolution process of pegmatite, based on the study of the geological characteristics of pegmatite, we carried out a whole-rock geochemical analysis of Ke'eryin two-mica granite and Lijiagou pegmatite and carried out a detailed electron probe microanalysis (EPMA) and laser ablation inductively coupled plasma mass spectrometry (LA-ICPMS) analysis of mica minerals in each zonal pegmatite. The results show that the Ke'eryin two-mica granite is mainly formed in the transition period from syn-collision to post-collision. After the end of the continental collision, the crust is squeezed and thickened in the post-collision extensional transition tectonic environment. Mica from the microcline pegmatite zone (MP) to the albite spodumene pegmatite zone (ASP) in pegmatite show different compositions and structural characteristics, with the evolution trend in the direction from muscovite to Li-bearing mica. The type of mica from MP to AP is mainly muscovite, and Li-bearing mica appears in ASP, which is secondary and metasomatic at the edge of primary muscovite. From MP to ASP, there was a negative correlation between Nb/Ta, K/Rb and the Li, Rb, and Cs contents of mica, while the contents of Li, Rb, Cs, and F in the Li-bearing mica of ASP increased sharply. This evidence illustrates that the favorable tectonic environment contributed to the formation of the Lijiagou pegmatitic spodumene deposit. Lijiagou pegmatite experienced the magmatic–hydrothermal evolution process and has a high degree of differentiation and evolution from MP to ASP, which gradually increased. Combined with the change in mica type, it is considered that ASP formed from the stage of magmatic transition to hydrothermal and was a hydrothermal environment, and Li, Rb, and Cs mainly began to enrich at the stage of magmatic–hydrothermal transition.

Keywords: geochemistry; mica; magmatic–hydrothermal evolution; Lijiagou pegmatite spodumene deposit; Songpan–Garze Fold Belt

Citation: Chen, X.; Chen, C.; Lai, X.; Yang, Y.; Gu, Y.; Cai, Y. Whole-Rock Geochemistry and Mica Compositions in Lijiagou Pegmatite Spodumene Deposit, Western Sichuan, China. *Minerals* **2024**, *14*, 69. https://doi.org/10.3390/min14010069

Academic Editor: Nikita V. Chukanov

Received: 17 October 2023
Revised: 19 December 2023
Accepted: 22 December 2023
Published: 5 January 2024

1. Introduction

Lithium (Li) is one of the most important rare-metal elements and the lightest metal element in nature. Because of its excellent physical and chemical properties, it is used in new energy, new materials, information technology, and aerospace fields. It is an indispensable strategic metal for the development of emerging industries and has important strategic significance for China and the rest of the world [1–4]. Granitic pegmatites are generally considered to be formed from highly differentiated, volatile-rich, residual granitic magma, which is of great economic significance because it contains various rare-metal elements such as Li, Be, Nb, Ta, Rb, Cs, W, and Sn [5–10]. Due to the high cost of mining salt lake Li resources, granite pegmatite Li deposits have become the main source of Li in China [11–13]. The evolution of granite pegmatite is a very complex process, and its degree of evolution determines the mineralization of rare-metal elements to a large extent.

The magmatic–hydrothermal transition stage in the evolution process is the beginning of the high enrichment of rare metals [14]. Granite pegmatite rare-metal deposits are the product of the magmatic–hydrothermal stage, ore-forming fluids mainly originate from highly differentiated granitic magmas, and the differentiation evolution process plays an important role in controlling diagenesis and mineralization [7]. Although pegmatite melt is mostly considered to be the residual melt produced by magma separation and the crystallization of mother granite [7,15–17], experimental studies have shown that fluid immiscibility is also a critical mechanism of rare-metal enrichment during magmatic evolution [18–20].

Mica is common in granitic pegmatite and is also an important rock-forming mineral in granitic pegmatite. They not only crystallize in the magmatic stage but are also partly involved in hydrothermal processes. As a phyllosilicate mineral, mica has a TOT layered structure, which can enable it to host many rare elements such as Li, Be, Rb, Cs, Ba, Sn, Nb, and Ta [21]. The type, texture, and chemical characteristics of mica can indicate the degree of evolution of pegmatite melt and the evolution process of pegmatite veins [22–26]. These characteristics make it a rare-metal carrier mineral and an indicator mineral for rare-metal mineralization. Therefore, a study of micas can provide constraints on the complex magmatic–hydrothermal processes related to rare-metal mineralization.

Lijiagou pegmatite spodumene deposit is located in central SGFB (proven resources of 0.51 Mt at 1.27% Li, 3696 t at 0.009% Nb, 1747 t at 0.004% Ta, 19,807 t at 0.049% Be, and 21,240 t at 0.052% Sn). The deposit is the third largest spodumene pegmatite deposit in Asia, after the Dangba (Li resources of 0.66 Mt) and Jiajika (Li resources of 0.92 Mt) deposits [27]. Previous studies of the Lijiagou pegmatite spodumene deposit have mainly focused on geological characteristics [28], the origin and characteristics of the fluid [19,27,29,30], the geochronology of pegmatite [31,32], the origin of pegmatite magmas, and their relationship with the Ke'eryin pluton granites [19]. In this paper, we selected representative samples of the Ke'eryin pluton and pegmatites from the Lijiagou deposit for a geochemical analysis of whole rock and mica and used these data to analyze the metallogenic tectonic environment characteristics and magmatic–hydrothermal evolution processes of pegmatites. These efforts aim to obtain a better understanding of the evolution of Lijiagou rare-metal pegmatite and facilitate the exploration of related granitic pegmatite deposits.

2. Geological Background

Lijiagou pegmatite spodumene deposit is located in Jinchuan County, western Sichuan Province (Figure 1a), situated in the southeastern part of the Ke'eryin pegmatite ore field, central Songpan–Garze Fold Belt. It is bounded by the Kunlun–Anyemaqen suture on the north, the Ganzi–Litang suture on the southwest, and the Longmenshan thrust on the southeast (Figure 1b). The area of the Lijiagou deposit covers approximately 4.35 km^2. It is dominated by metasedimentary rocks of the Triassic Xikang Group, which mainly comprise gray, black meta-felsic sandstone, meta-siltstone, sericite slate, silty slate, phyllite, schist, and minor limestone [33]. The metasedimentary rocks show characteristics of high-temperature and middle–low-pressure metamorphism, forming zonal patterns with sillimanite–kyanite, garnet–staurolite, and biotite–andalusite zones from core to periphery [34]. Folds and faults are well-developed in this area, which was influenced by the late Indosinian orogeny; many NW- and WNW-trending folds developed while NE-striking reverse faults resulted from a horizontal compressive stress field in the Jurassic Yanshan orogeny [35,36]. The magmatic rocks in the region are mainly exposed to two-mica granite with a wide distribution range and a total outcrop area of 188 km^2, which intruded into the Triassic Xikang Group strata from around 231 to 200 Ma [31,37] and caused different degrees of thermodynamic contact metamorphism. Some rare-metal pegmatite deposits are distributed around the Ke'eryin two-mica granite pluton, including Guanyinqiao, Lijiagou, Dangba, Yelonggou, Simancuo, Sizemuzu, and Redamen deposits (Figure 1c). The maximum width of these pegmatite dikes is 30 m, and the longest reaches up to 2200 m [38]. The pegmatite dikes have a zonal distribution in the horizontal directions from the Ke'eryin granite pluton outwards. Based on their mineral composition, the pegmatite dikes can be divided into five types (Figure 1c), with increasing distance from the Ke'eryin granite pluton, which are: (I) microcline pegmatite (MP), (II) microcline albite pegmatite (MAP), (III) albite pegmatite (AP), (IV) albite spodumene pegmatite (ASP) and (V) lepidolite pegmatite (LP) [39]. The vertical partition of pegmatite is imperfect, and some pegmatite types overlap. A single pegmatite body may contain two or three types of pegmatite.

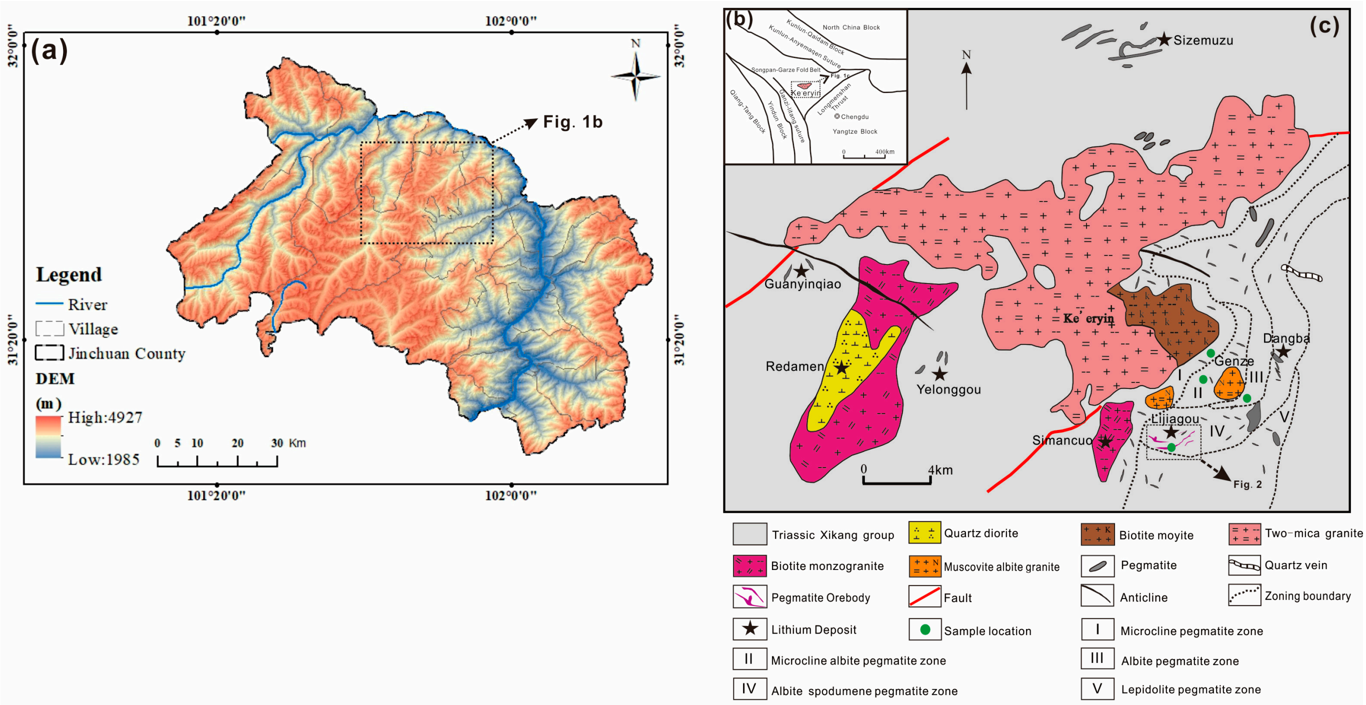

Figure 1. (**a**) Geographical location of Jinchuan County; (**b**) tectonic position of Ke'eryin (modified from [40]); (**c**) geological sketch map of Ke'eryin area (modified from [31,40]).

Lijiagou deposit outcrops in the Upper Triassic Zhuwo Formation (T_3zh). The joint fissures are well-developed, which are EW, WNW-ESE, and NW-SE trending joint fissures, and are mainly related to the ore-bearing granitic pegmatite. Aplite dikes have mainly been identified in and near the Lijiagou deposit from both drilling and field exploration. However, based on analyses of the zircon and monazite U-Pb ages, zircon Hf and monazite Nd isotopes, whole-rock and mineral chemical data, Fei et al. proposed that aplite does not have rare-metal mineralization potential [41]. Approximately 85 pegmatite veins are exposed in the Lijiagou deposit and 15 ore bodies have been identified (I–X, XI (XI-1, XI-2, XI-3, XI-4, XI-5), XII, XIII, XIV and XVI) (Figure 2). These are mainly veins, such as No. I and II, with tabular or lenticular shapes. The No. I pegmatite is the largest orebody. It is a vein-shaped body with a predominant NE orientation and is 10–124 m thick, 375 m deep, and 2060 m long [34].

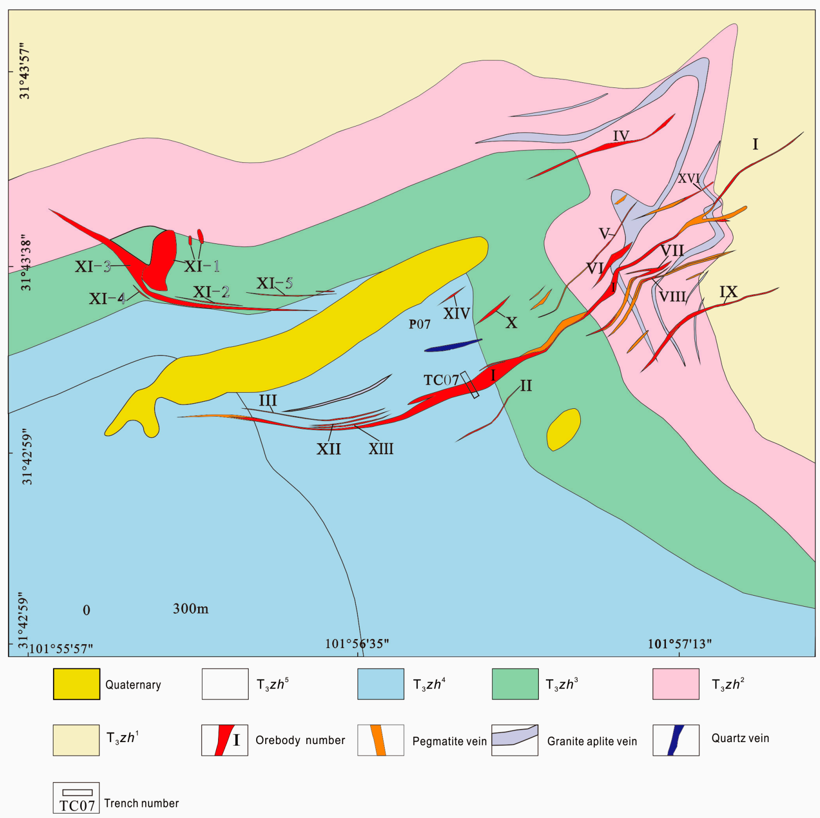

Figure 2. Geological map of Ljiagou spodumene deposit (modified from [27]).

3. Sample and Petrographic Characteristics

In the Ke'eryin ore field, pegmatites can be divided into the barren pegmatites (I-MP, II-MAP, III-AP) and the ore-bearing pegmatites (IV-ASP). In this study, samples of two-mica granite were collected from the southeastern branch of Ke'eryin pluton for whole-rock geochemical analysis. The barren pegmatite samples were collected from outcrops and ore-bearing pegmatite samples were taken from the drill core of No. I orebody in Lijiagou deposit for whole-rock and mica geochemical analysis. The two-mica granite is mainly gray, ranges from fine to medium-grained, and is composed of K-feldspar, plagioclase, quartz, biotite, and muscovite. Some characteristics of the pegmatite samples are described in Section 3.1.

3.1. Petrographic Characteristics of the Pegmatite

The MP, MAP, AP, and ASP all have outcrops in the field (Figure 3a,d,g,j), while LP has few outcrops and only appears locally. The ASP is the main type, with minor AP in the Lijiagou deposit. The MP intruded into two-mica granite and biotite moyite. The MAP, AP, and ASP mainly intruded into metasedimentary rocks. MP and MAP have a similar composition (Figure 3b,c,e,f), being mainly composed of microcline, albite, quartz, muscovite, biotite, tourmaline and a small amount of garnet, while MP has a higher content of microcline. The AP exhibit a weaker internal zonation than the MP and MAP. It is mainly composed of albite, muscovite, and quartz (Figure 3h,i). The main spodumene-bearing pegmatite is ASP. They consist of albite, spodumene, quartz, muscovite and small amounts of columbite (Figure 3k,l). The U-Pb ages of coltan and cassiterite might represent the crystallization time for pegmatite during the magmatic stage [42–44]. According to the columbite–tantalite U-Pb geochronology, the ASP in the Lijiagou deposit was formed at ±211.1 Ma [31].

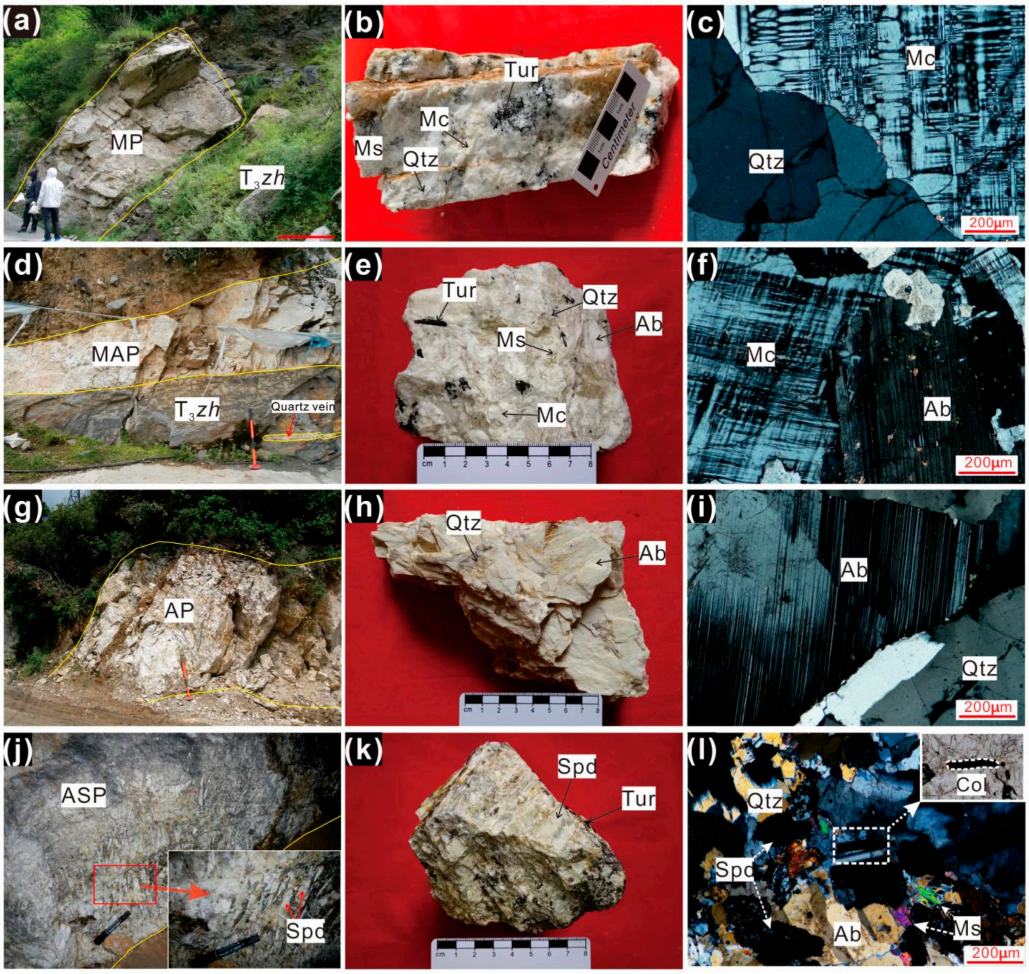

Figure 3. Photographs of outcrops, hand specimens and microscope images of various types of pegmatite from the Lijiagou area; (**a**–**c**) photographs from microcline pegmatite; (**d**–**f**) photographs from microcline albite pegmatite; (**g**–**i**) photographs from albite pegmatite; (**j**–**l**) photographs from albite spodumene pegmatite. MP: microcline pegmatite; MAP: microcline albite pegmatite; AP: albite pegmatite; ASP: albite spodumene pegmatite; Mc: microcline; Qtz: quartz; Ms: muscovite; Tur: tourmaline; Ab: albite; Spd: spodumene; Col: columbite.

3.2. Mineralogical Characteristics of Micas

Micas exists in each zone as a penetrative mineral and presents a change in texture from the MP to ASP zone, while muscovite–Li-bearing mica series are the main constituents of the micas from Lijiagou pegmatites. The mica types have a similar texture in the barren pegmatites (from the MP to AP zone) of the Lijiagou area, which are mainly muscovite, with a wide range of particle sizes ranging from the micrometer to millimeter level, and often occur in a semi-euhedral to euhedral flake symbiosis with albite or quartz (Figure 4a–f). The muscovite shows no zoning in BSE images (Figure 4j,k). However, the type of micas has changed in rocks of the ore-bearing pegmatite (ASP zone), where it occurs in both primary and secondary forms. Primary muscovite generally appears as a large flake with curved cleavages (Figure 4g), and does not show bright and dark domains in high-contrast BSE images (Figure 4l), indicating that it is chemically homogeneous. Li-bearing mica occurs sporadically as a secondary form around primary muscovite or along cleavage planes, and is brighter than muscovite in high-contrast BSE images (Figure 4m–o). Secondary Li-bearing mica is smaller than primary muscovite and commonly fills interstitial spaces between spodumene and primary muscovite (Figure 4h). This may be the result of the migration of ore-forming fluids along mineral gaps and the metasomatism of primary minerals (Figure 4i).

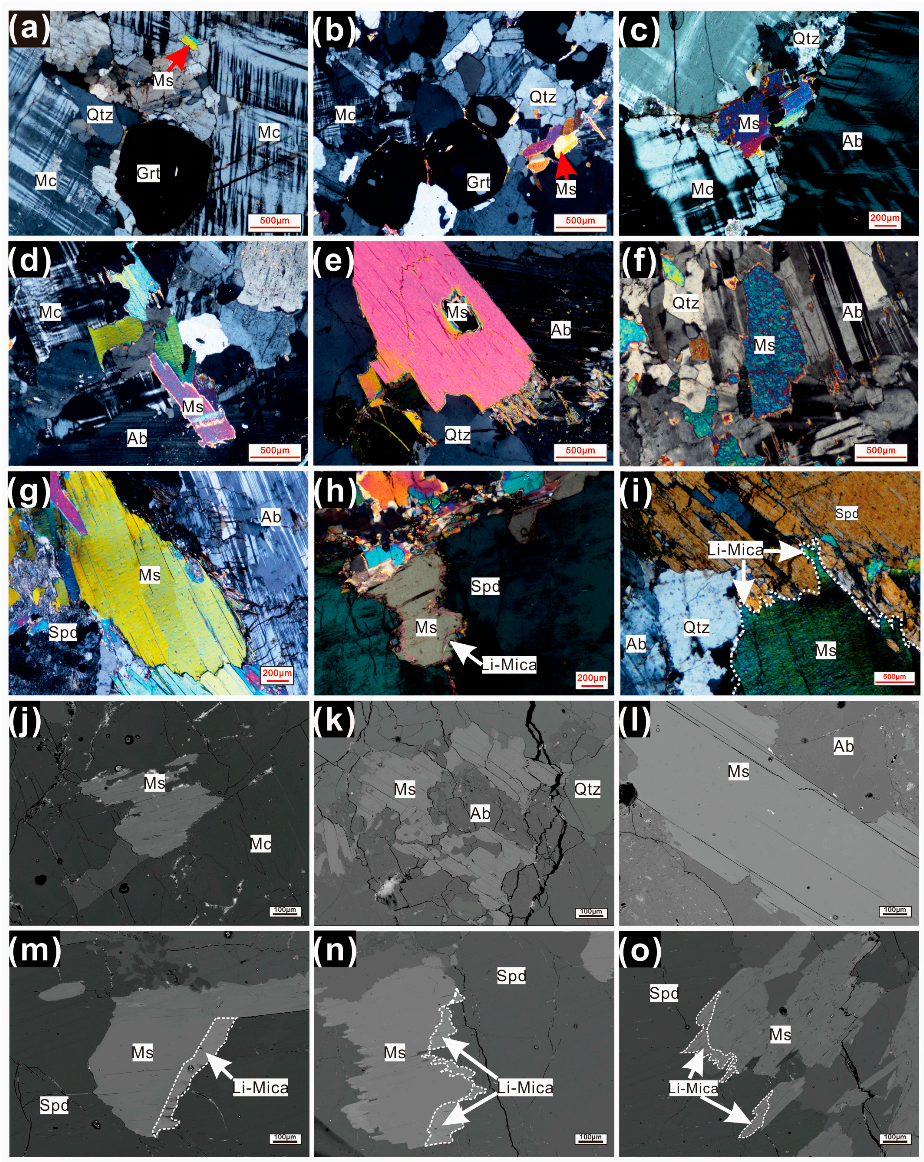

Figure 4. BSE images and micrographs of micas in different types of pegmatite in the Lijiagou area. (**a**–**f**) Micrographs of muscovite in barren pegmatites; (**g**) micrographs of muscovite in ore-bearing pegmatite; (**h**,**i**) micrographs of Li-bearing mica in ore-bearing pegmatite; (**j**–**l**) BSE images of muscovite in barren pegmatites; (**m**–**o**) BSE images of Li-bearing mica in ore-bearing pegmatite. Mc—microcline; Qtz—quartz; Ms—muscovite; Grt—garnet; Ab—albite; Spd—spodumene; Li-Mica—Li-bearing mica.

4. Analytical Methods

4.1. Whole-Rock Analysis

The whole-rock major, trace, and rare-earth elements were analyzed at the China In-stitute for Multipurpose Utilization of Mineral Resources, CAGS. The rock samples were crushed to a centimeter level, and fresh samples without alteration were selected. The sample was then crushed into a powder of less than 200 mesh for further analysis. For the analysis of the major elements, 0.5 g of the sample, 5.0 g of the cosolvent ($Li_2B_4O_7$), and 0.3 g of the crucible protectant (NH_4NO_3) were weighed and mixed well. After adding 1~2 drops of LiBr, the mixture was melted in a heating furnace. After cooling, the molten glass was analyzed by inductively coupled plasma optical emission spectrometer (ICP-OES, PE 5300V, Perkinelmer, Inc., Waltham, Massachusetts, USA), and the analysis error was less than 1%. For the analysis of trace elements, 50.00 mg ($\pm$0.50 mg) of samples with a particle size of less than 75 µm were accurately weighed and placed in a polytetrafluoroethylene (PTFE) tank. A total of 1.0 mL HF and 0.5 mL HNO_3 were added and shaken. After that, the mixture was placed on an electric heating plate at 140 °C and evaporated to dryness. Finally, the trace elements in the samples were analyzed by inductively coupled plasma mass spectrometry (ICP-MS, Agilent 7700, Agilent Technologies Inc., Santa Clara, California, USA). The analysis error of most trace elements was less than 5%, and the analysis error of some volatile elements and very low contents of these elements was less than 10% [45,46].

4.2. EPMA Analysis

Major element analyses of muscovite were carried out at the Electron Probe Laboratory, School of Earth Science and Technology, Southwest Petroleum University. Using a JEOL-JXA-8230(Shimadzu, Inc., Kyoto City, Japan) electron microprobe equipped with EDAX-GENESIS Energy dispersive spectroscopy (Shimadzu, Inc., Kyoto City, Japan). The electron probe analysis was carried out under the conditions of an accelerating voltage of 15 kV and an accelerating current of 20 nA, and the selected beam spot diameter was 10 µm. All test data were corrected by ZAF. The measurement time of the characteristic peaks of Na, Mg, K, Ca, Fe, Ti, Al, Si, Ni, Cr, and Mn elements was 10 s, and the measurement time of the upper and lower background was half of the characteristic peak measurement time, respectively.

4.3. LA-ICPMS Analysis

In situ trace element analyses of muscovite were carried out using a laser ablation inductively coupled–plasma mass spectrometer at the FocuMS Technology Co. Ltd., Nanjing, China. An Agilent 7700× ICP-MS instrument (Agilent Technologies Inc., Santa Clara, CA, USA) was coupled with a Teledyne Cetac Technologies 193 nm ArF excimer laser ablation system. For this sample analysis, the laser beam spot size was 44 µm and the frequency was 5 Hz. Standard materials BIR-1G, BCR-2G, and BHVO-2G were used for multi-external standard calibration without internal standard correction [47]. Finally, the measured data were processed offline by the software ICPMS DataCal 12.2 [47]. The analytical uncertainties are 5%–10% for trace elements and generally better than 5% for major elements. The analytical uncertainties are 5%–10% for trace elements and generally better than 5% for major elements.

5. Results

5.1. Whole-Rock Geochemistry

The major element composition of the Ke'eryin granite pluton and Lijiagou pegmatites are shown in Table 1. The average content of Al_2O_3 in two-mica granite (average 15.5 wt%) is slightly higher than that in barren pegmatite (average 14.09 wt%) and ore-bearing pegmatite (average 14.57 wt%). The average content of CaO (average 1.39 wt%) in two-mica granite is higher than that in barren pegmatite (average 0.49 wt%) and ore-bearing pegmatite (average 0.32 wt%). The content of P_2O_5 in two-mica granite (0.11–0.33 wt%) is not very different from that in barren pegmatite (0.07–0.35 wt%), but the content of P_2O_5 in ore-bearing pegmatite (0.22–0.78 wt%) is significantly higher. The increase in P content in the melt often reflects the enrichment of rare-metal elements [48,49]. The Na_2O/K_2O ratio of two-mica granite ranges from 0.42 to 0.79, with an average of 0.62, and the K content is greater than the Na content, indicating that it is a potassium-rich granite. The $Na_2O + K_2O$ values of two-mica granites range from 7.83 to 8.56 wt%, those of barren pegmatite from 8.21 to 8.83 wt%, and the values of ore-bearing pegmatite range from 5.24 to 7.40 wt%, which is significantly lower.

The differentiation index (DI) of the two-mica granite and the pegmatite, with an average value of 92.06, generally shows the characteristics of highly differentiated granitic magma. In the TAS diagram (Figure 5a), Lijiagou pegmatite and two-mica granite drop points basically fall into the granite area. In the A/NK-A/CNK diagram (Figure 5b), the two-mica granite and pegmatite samples fall into the peraluminous area. The A/CNK of the two-mica granite is 1.42–1.74, and the barren pegmatite is 1.32–2.69. The A/NK and A/CNK indexes of the ore-bearing pegmatite are generally higher than those of the two-mica granite and the barren pegmatite. In the K_2O-SiO_2 diagram, the two-mica granite and barren pegmatite show high-potassium calc-alkaline characteristics, and the ore-bearing pegmatite is biased towards medium-to-low-potassium calc-alkaline characteristics (Figure 5c). The Rittmann index (σ43) of granite and pegmatite ranges from 0.85 to 2.90, both of which are less than 3.3, indicating that they are calc-alkaline series rocks. In the alkalinity rate diagram (Figure 5d), both the two-mica granite and the barren pegmatite fall into the alkaline area, and a few ore-bearing pegmatites are calc-alkaline, which is different from the characteristics of the Rittman index. This may be attributed to the inherent complexity of the magma source or the assimilation and contamination of the surrounding rock during the evolutionary process. In summary, the two-mica granite is a high-potassium, alkaline–calcium, alkaline, strongly peraluminous granite, and Lijiagou pegmatite is an alkaline–calcium, alkaline, strongly peraluminous granite pegmatite.

The trace and rare-earth element compositions of the Ke'eryin granite pluton and Lijiagou pegmatites are shown in Table 2. The Li content in the two-mica granite is 93–211 ppm, the barren pegmatite of the Lijiagou deposit is 36–446 ppm, and the ore-bearing pegmatite can reach 9353–11,176 ppm. The content of Be in the two-mica granite is 4.31–6.46 ppm, the barren pegmatite of the Lijiagou deposit is 9.27–160.53 ppm, and the ore-bearing pegmatite is 184.99–399.64 ppm. The Rb content in the two-mica granite is 251–289 ppm, the barren pegmatite of the Lijiagou deposit is 320–982 ppm, and the ore-bearing pegmatite is 496–1120 ppm. In the spider diagram of trace elements (Figure 6a), large-ion lithophile elements such as Ba and Sr in pegmatite generally show negative anomalies due to loss, and Ba and Sr in two-mica granite also show negative anomalies. The LREE/HREE of the two-mica granite is 7.50–16.55, which is characterized by the enrichment of light rare-earth elements and relative loss of heavy rare-earth elements.

Table 1. Major-element compositional variations in the Ke'eryin granite pluton and Lijiagou pegmatite.

	(Ke'eryin Pluton) Two-Mica Granite		(Barren Pegmatite) MP–MAP–AP		(Ore-Bearing Pegmatite) ASP	
	Min–Max	**Avg**	**Min–Max**	**Avg**	**Min–Max**	**Avg**
SiO_2 (wt%)	68.06–73.61	72.09	73.14–77.52	74.8	68.68–75.29	71.70
TiO_2 (wt%)	0.05–0.36	0.16	-	-	0.01–0.04	0.02
Al_2O_3 (wt%)	14.37–15.97	15.15	12.08–15.11	14.09	13.43–16.91	14.57
Fe_2O_3 (wt%)	0.16–2.59	0.66	0.31–0.7	0.45	0.27–0.62	0.45
MnO (wt%)	0.02–0.22	0.06	0.02–0.37	0.15	0.07–0.36	0.15
MgO (wt%)	0.03–0.70	0.25	0.01–0.04	0.03	0.01–0.2	0.09
CaO (wt%)	0.95–2.62	1.39	0.34–0.6	0.49	0.2–0.4	0.32
Na_2O (wt%)	2.50–3.59	3.13	2.66–7.17	3.86	1.98–5.32	4.06
K_2O (wt%)	4.03–6.01	5.16	1.03–6.17	3.86	0.97–3.27	2.60
P_2O_5 (wt%)	0.11–0.33	0.17	0.07–0.35	0.20	0.22–0.78	0.47
LOI	0.32–1.17	0.68	0.33–1.09	0.74	0.5–0.69	0.59
$Na_2O + K_2O$	7.83–8.56	8.30	8.21–8.83	8.58	5.24–7.4	6.66
Na_2O/K_2O	0.42–0.79	0.62	0.43–6.94	2.78	0.61–5.19	2.04
DI	81.32–92.65	89.71	94.71–97.52	95.71	88.84–94.64	92.57
σ43	2.00–2.90	2.37	2.22–2.44	2.31	0.85–2.05	1.56
AR	2.73–3.43	3.04	3.19–5.92	4.21	2.03–3.36	2.73
R1	2174–2817	2505.70	2097–2790	2423.30	2367–3616	2862.80
R2	406–633	466.67	277–367	334.67	321–381	343.17
A/NK	1.71–1.96	1.83	1.37–1.84	1.65	1.8–2.88	2.24
A/CNK	1.42–1.74	1.57	1.32–1.72	1.56	1.73–2.69	2.13

Min–Max: minimum value–maximum value; avg: average value; $σ43 = (Na_2O + K_2O)^2/(SiO_2 - 43)$; $AR = [Al_2O_3 + CaO + (Na_2O + K_2O)]/[Al_2O_3 + CaO - (Na_2O + K_2O)]$; $R1 = 4Si - 11(Na + K) - 2(Fe + Ti)$; $R2 = 6Ca + 2Mg + Al$; $A/NK = (Al_2O_3/(Na_2O + K_2O))$; $A/CNK = (Al_2O_3/(CaO + Na_2O + K_2O))$; MP—microcline pegmatite; MAP—microcline albite pegmatite; AP—albite pegmatite; ASP—albite spodumene pegmatite.

Table 2. Trace and rare-earth element compositional variations in the Ke'eryin granite pluton and Lijiagou pegmatite.

	(Ke'eryin Pluton) Two-Mica Granite		(Barren Pegmatite) MP–MAP–AP		(Ore-Bearing Pegmatite) ASP	
	Min–Max	**Avg**	**Min–Max**	**Avg**	**Min–Max**	**Avg**
Li (ppm)	93–211	149.00	36–446	228.00	9353–11,176	10,264.5
Be (ppm)	4.31–6.46	5.19	9.27–160.53	59.06	184.99–399.64	292.32
Sn (ppm)	5.21–16.5	9.00	12.6–295.5	120.45	258.55–266.27	262.41
Cs (ppm)	13.5–19.4	16.60	40.6–83.2	58.70	148.8–191.1	169.95
Ga (ppm)	16.9–22.4	19.38	13.5–27.5	21.80	12.3–19.5	15.9
Se (ppm)	0.03–0.66	0.19	0.03–0.06	0.04	0–0.03	0.03
Rb (ppm)	251–289	270.75	320–982	738.33	496–1120	808
Ba (ppm)	158–1669	1004.25	5.92–24.53	13.37	0.69–2.69	1.69
Th (ppm)	10.2–20.8	17.60	0.39–1.9	0.94	0.08–2.31	1.2
U (ppm)	2.74–8.01	5.04	0.51–31.4	10.85	5.53–14.83	10.18
Ta (ppm)	1.08–3.08	1.82	3.83–11.26	8.41	57.39–87.82	72.61
Nb (ppm)	10.67–20.6	15.97	11.73–49.67	32.87	141.31–185.48	163.4
Sr (ppm)	60.2–335	224.51	9.62–52.52	25.32	0.95–1.68	1.32
Zr (ppm)	58.3–164	123.66	3.8–25.52	12.94	5.76–16.12	10.94
Hf (ppm)	2.32–4.32	3.69	0.15–1.4	0.65	0.47–1.73	1.1
Yb (ppm)	1.14–1.56	1.32	0.01–0.22	0.14	0.01	0.01
Y (ppm)	17.1–18.2	17.77	0.1–1.49	0.84	0.15–0.24	0.2
K/Rb	154.47–198.69	166.90	26.71–56.08	39.96	14.30–24.15	19.27
Zr/Hf	25.13–38.68	32.61	18.22–24.58	21.96	9.34–12.25	10.80
Nb/Ta	6.69–12.31	9.51	3.06–4.41	3.71	1.61–3.23	2.42
La (ppm)	16.9–54.9	38.88	0.05–0.64	0.42	0.11–0.22	0.16
Ce (ppm)	34.5–102	71.05	0.09–1.22	0.83	0.13–0.32	0.23
Pr (ppm)	4.21–12.5	8.68	0.01–0.13	0.08	0.01	0.01
Nd (ppm)	17.1–50.4	33.55	0.01–0.42	0.26	0.01	0.01
Sm (ppm)	4.38–8.91	6.21	0–0.19	0.10	-	-
Eu (ppm)	0.55–2.1	1.44	0.01–0.02	0.02	-	-
Gd (ppm)	3.68–6.05	5.03	0.01–0.18	0.09	0.01	0.01
Tb (ppm)	0.6–0.79	0.68	0–0.04	0.02	-	-
Dy (ppm)	2.34–3.36	3.05	0.01–0.25	0.13	0.01–0.03	0.02
Ho (ppm)	0.6–0.62	0.61	0–0.04	0.02	-	-
Er (ppm)	1.49–1.78	1.64	0.01–0.11	0.07	0.01–0.02	0.01
Tm (ppm)	0.2–0.25	0.23	0–0.02	0.02	-	-
Yb (ppm)	1.14–1.56	1.32	0–0.22	0.14	0.01	0.01
Lu (ppm)	0.17–0.23	0.21	0–0.04	0.02	-	-
∑REE	87.99–244.76	172.58	0.19–3.43	2.21	0.36–0.61	0.48
∑LREE	77.64–230.81	159.80	0.17–2.57	1.71	0.26–0.57	0.42
∑HREE	10.35–13.97	12.77	0.03–0.86	0.50	0.1–0.04	0.07
LREE/HREE	7.5–16.55	12.22	2.97–6.7	4.51	2.78–13.86	8.32
La_N/Yb_N	10.63–30.29	20.88	2.04–7.61	3.92	5.25–11.02	8.14
δEu	0.41–0.97	0.73	0.34–6.41	2.48	0.18–0.57	0.37
δCe	0.82–0.98	0.92	0.99–1.17	1.06	0.86–1	0.93

Min–Max: minimum value–maximum value; avg: average value.

The LaN/YbN of the two-mica granite is 10. 63–30.29, indicating fractionation between light and heavy rare-earth elements, and the δEu is 0.41–0.97, showing a weak–medium negative Eu anomaly. The δCe of the two-mica granite is 0.82–0.98, and the cerium anomaly is slight or not obvious. The ∑REE abundance value of the two-mica granite is 87.99–244.76 ppm. Compared with the two-mica granite, the ∑REE abundance value in the pegmatite is greatly reduced, only 0.19–3.43 ppm. In the rare-earth element distribution diagram (Figure 6b), it can also be seen that the distribution curve of the pegmatite is located below the two-mica granite. Compared with the LREE/HREE and La_N/Yb_N ratios of the two-mica granite, the LREE/HREE in the pegmatite is 2.78–13.86, and the La_N/Yb_N is 2.04–11.02. The ratio is significantly reduced, indicating that the fractionation of light and heavy rare earths is relatively weak at this time, and then the ratio tends to increase.

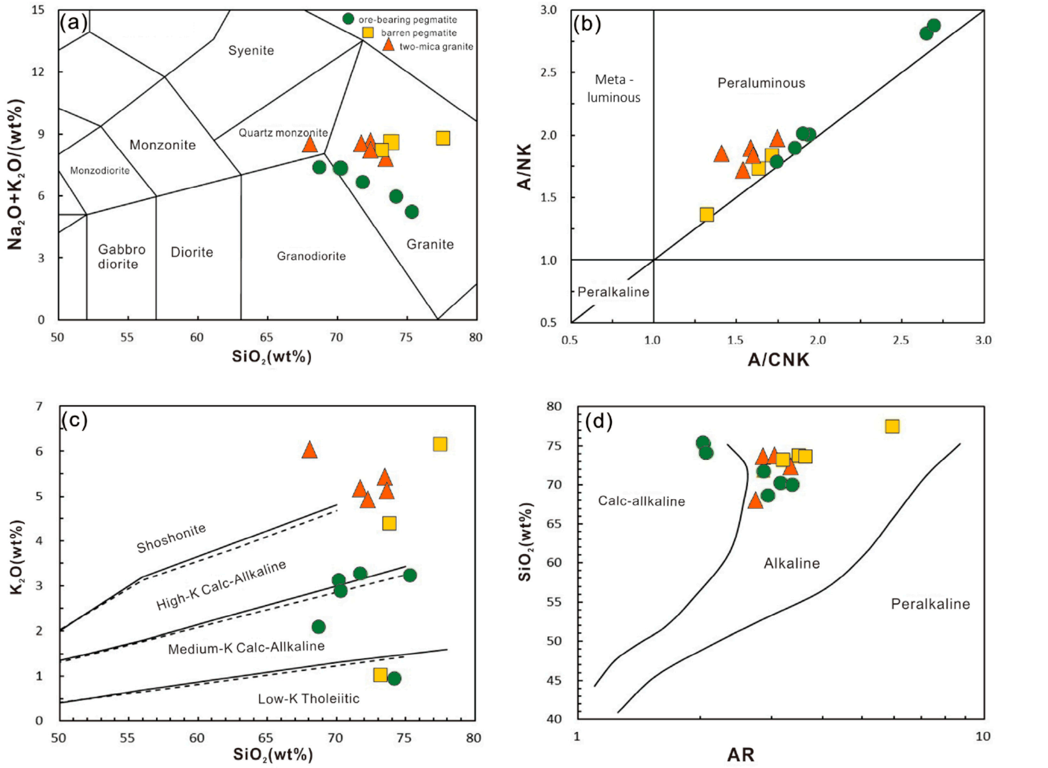

Figure 5. Major element diagrams of the Ke'eryin granite pluton and Lijiagou pegmatite. (**a**) Total alkali versus silica diagram [50]; (**b**) A/NK vs. A/CNK diagram after [51]; (**c**) SiO_2 vs. K_2O diagram [52]; (**d**) alkalinity ratio variation diagram [53].

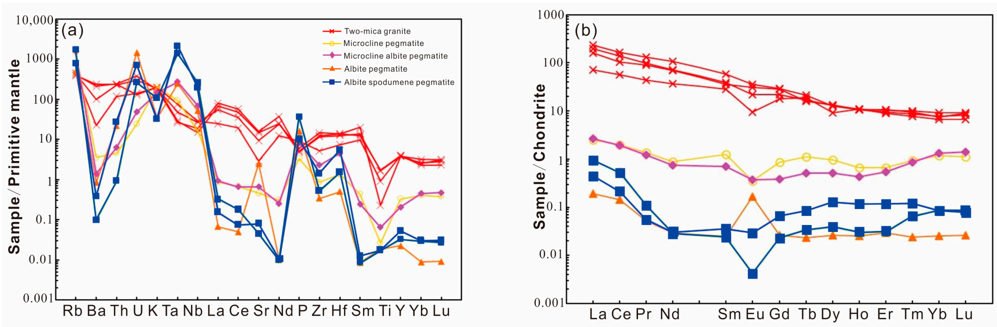

Figure 6. (**a**) Primitive mantle-normalized incompatible element distribution patterns and (**b**) Chondrite-normalized REE distribution patterns of the Ke'eryin granite pluton and Lijiagou pegmatite. Normalization values are taken from [54].

5.2. Major and Trace Element Compositions of Muscovite

The major and trace element compositions of micas from Lijiagou pegmatite are summarized in Table 3. In terms of the composition of major elements, except for the similar K_2O content (average 10.29–11.01 wt%), the changes in other elements show regularity (Figure 7). The contents of SiO_2 (45.55–46.97 wt%), Al_2O_3 (35.72–38.15 wt%), FeO (1.66–2.11 wt%), MnO (0.02–0.11 wt%), MgO (0.29–0.51 wt%), TiO_2 (0.03–0.07 wt%) and F (0.38–0.62 wt%) in muscovite from MP and MAP are similar. The contents of Al_2O_3 (35.83–37.64 wt%) and MgO (0.32–0.44 wt%) in muscovite of AP are lower than those in MP and MAP. The contents of SiO_2 (45.66–46.97 wt%) and F (0–1.91 wt%) are higher than those in MP and MAP. Compared with the content of SiO_2 (44.62–47.80 wt%), Al_2O_3 (33.32–37.49 wt%), FeO (0.64–3.96 wt%) MnO (0.07–0.58 wt%) and F (0.44–5.86 wt%) in Li-bearing mica (low Li content) of ASP. The Li-bearing mica (high Li content) in ASP has lower Al_2O_3 (21.14–23.21 wt%) and higher SiO_2 (48.72–50.55 wt%), FeO (5.79–6.46 wt%), MnO (0.53–1.59 wt%) and F (8.94–10.87 wt%). According to the EPMA analysis results, the empirical chemical formula calculated based on 10 O atoms and 2 additional anions, the formula of muscovite from MP-AP is close to KAl_2 (Si_3AlO_{10}) $(OH)_2$, and the formula of Li-bearing mica(high Li content) from ASP is $(K_{0.85}Na_{0.01})$ $(Al_{0.86}Fe_{0.33}Mn_{0.05}Li_{0.63})$ $(Si_{3.17}Al_{0.83}O_{10})$ $F_{2.02}$, which may be Fe-rich luanshiweiite [55,56].

Table 3. Major and trace element compositions of micas from the Lijiagou pegmatite.

Type	Value	wt%								
		SiO_2	TiO_2	Al_2O_3	FeO	MnO	MgO	Na_2O	K_2O	F
I	Avg	45.93	0.06	36.57	1.78	0.06	0.43	0.37	11.01	0.52
	Min	45.93	0.04	35.98	1.71	0.03	0.33	0.29	10.82	0.41
	Max	46.31	0.07	36.83	1.87	0.1	0.51	0.43	11.3	0.62
II	Avg	46.21	0.05	36.04	1.88	0.05	0.37	0.4	10.84	0.46
	Min	45.55	0.03	35.72	1.66	0.02	0.29	0.28	10.52	0.38
	Max	46.76	0.07	36.66	2.11	0.11	0.49	0.56	11.13	0.56
III	Avg	46.4	0.02	36.59	1.57	0.07	0.38	0.31	10.48	0.98
	Min	45.66	0	35.83	1.24	0	0.32	0.16	10.08	0
	Max	46.97	0.07	37.64	1.91	0.14	0.44	0.39	11.22	1.91
IV	Avg	45.66	0.02	34.7	2.65	0.28	0.01	0.34	10.29	2.05
	Min	44.62	0	33.32	0.64	0.07	0	0.15	8.55	0.44
	Max	47.8	0.06	37.49	3.96	0.58	0.03	0.52	10.86	5.86
IV *	Avg	49.46	0.01	22.43	6.1	0.88	0.01	0.11	10.39	9.96
	Min	48.72	0	21.14	5.79	0.53	0	0.08	10.24	8.94
	Max	50.55	0.03	23.21	6.46	1.59	0.03	0.14	10.64	10.87

Type	Value	ppm								K/Rb	Nb/Ta
		Li	Be	B	Rb	Cs	Nb	Ta	Sn		
I	Avg	299.17	14.64	118.32	1163.6	54.72	191.98	23.27	194.47	80.05	8.37
	Min	273.74	11.04	109.21	980.68	45.44	167.09	20.30	167.27	68.74	6.13
	Max	326.07	18.79	126.19	1354.68	67.11	210.79	27.25	228.38	95.64	9.9
II	Avg	941.99	22.75	121.44	2205.11	97.57	265.62	53.26	417.93	41.11	5.24
	Min	869.61	21.66	113.03	2088.68	93.17	246.51	32.85	385.96	39.35	4.52
	Max	1027.76	24.24	131.18	2297.73	101.57	288.50	63.02	453.43	42.02	7.92
III	Avg	1961.49	20.2	173.01	5673.41	657.63	111.01	71.00	510.16	15.52	1.69
	Min	1603.77	18.09	118.07	3922.32	325.81	65.40	30.26	401.81	13.64	1.12
	Max	2466.98	23.2	211.24	6343.63	866.97	176.10	115.69	723.67	21.57	2.63
IV	Avg	4469.80	24.63	187.10	5630.59	693.80	141.55	44.37	540.22	15.77	3.35
	Min	2444.11	18.71	132.22	4735.45	225.95	14.85	10.07	453.21	13.08	1.06
	Max	7317.67	33.71	223.94	7051.88	1265.15	239.92	157.16	635.85	18.93	7.95
IV *	Avg	24,480.34	16.33	22.19	8733.76	1708.60	121.87	47.15	171.07	10.34	4.25
	Min	23,241.02	13.05	15.21	7780.91	1240.91	38.37	5.47	134.69	9.76	2.02
	Max	25,646.55	21.65	28.47	9303.18	1974.36	222.22	103.78	212.3	11.64	6.47

Min–Max: minimum value–maximum value; Avg: average value. I: muscovite in microcline pegmatite; II: muscovite in microcline albite pegmatite; III: muscovite in albite pegmatite; IV: Li-bearing mica (low Li content) in albite spodumene pegmatite; IV *: Li-bearing mica (high Li content) in albite spodumene pegmatite.

In terms of trace element composition, the contents of Li, Rb, and Cs in micas show regular characteristics, and their variation ranges are 273.74–25,646.55 ppm, 980.68–9303.18 ppm, and 45.44–1974.36 ppm, respectively, showing a gradual increase from MP to ASP. Among these elements, Li, Rb, and Cs reached their highest value in ASP. In addition, from MP to MAP, the content of Nb in muscovite gradually increased (164.09–288.5 ppm, average 228.8 ppm), but from AP to ASP, the content of Nb in muscovite and Li-bearing mica began to decrease (14.85–239.92 ppm, average 187.22 ppm), while the content of Ta in each type of pegmatite varies less (with an average content 23.27–71 ppm).

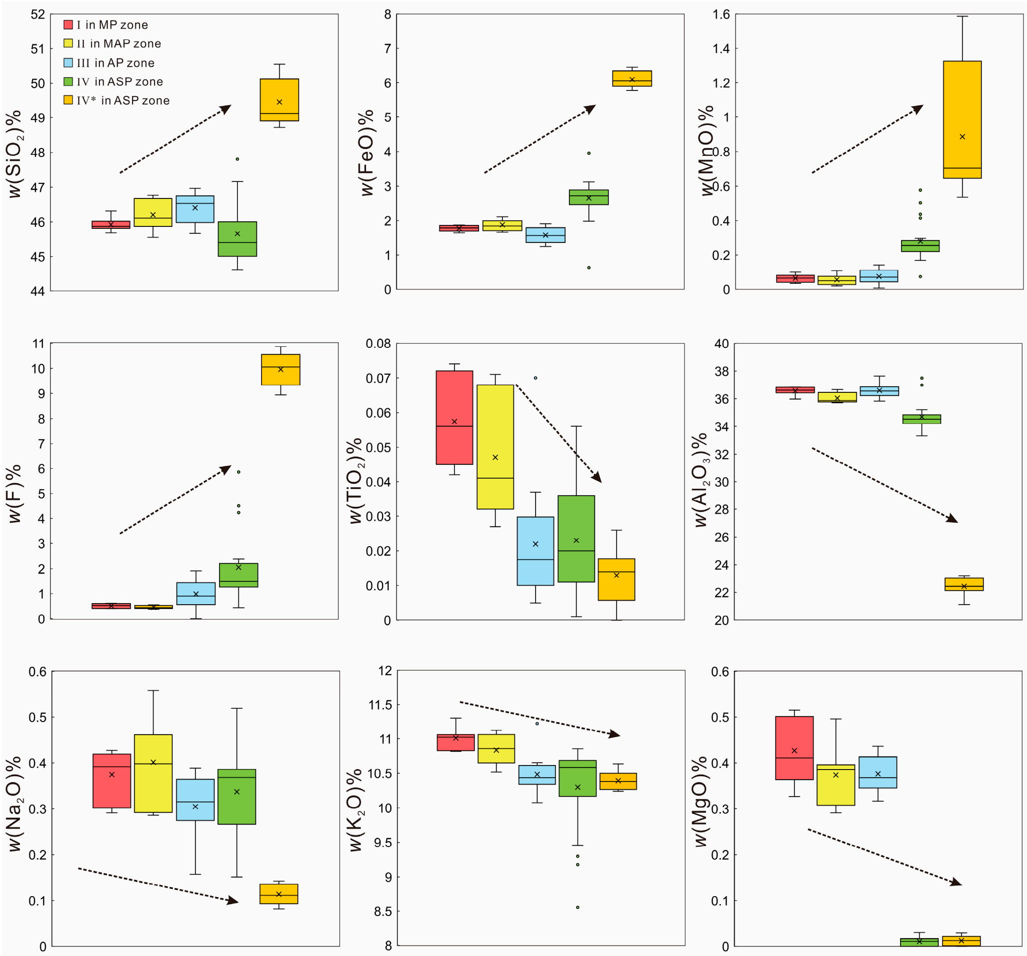

Figure 7. Box plots of major element changes in micas from Lijiagou pegmatite. I: muscovite in microcline pegmatite; II: muscovite in microcline albite pegmatite; III: muscovite in albite pegmatite; IV: Li-bearing mica (low Li content) in albite spodumene pegmatite; IV *: Li-bearing mica (high Li content) in albite spodumene pegmatite. MP—microcline pegmatite; MAP—microcline albite pegmatite; AP—albite pegmatite; ASP—albite spodumene pegmatite.

6. Discussion

6.1. Tectonic Environment

The formation of peraluminous granites is generally related to the continental collision environment, while strongly peraluminous granites are generally formed in the post-collision environment. In the Ta-Yb discriminant diagram (Figure 8a), the two-mica granite exhibits the characteristics of volcanic arc granite (VAG) and syn-collision granite (syn-COLG). In the Rb-(Nb + Y) discrimination diagram (Figure 8b), the two-mica granite falls into the region of post-collision granite (post-COLG). In the Rb-Hf-Ta discrimination diagram (Figure 8c), the plot point of the two-mica granite is close to the boundary transition position from the syn-COLG to post-COLG. In the R2-R1 discriminant diagram (Figure 8d), the two-mica granite transitioned from syn-collision to post-orogenic. Therefore, it is concluded that the Ke'eryin two-mica granite was mainly formed during the transition period from syn-collision to post-collision. That is, after the end of continental collision, the crustal compression thickened to the post-collision extensional transition tectonic environment.

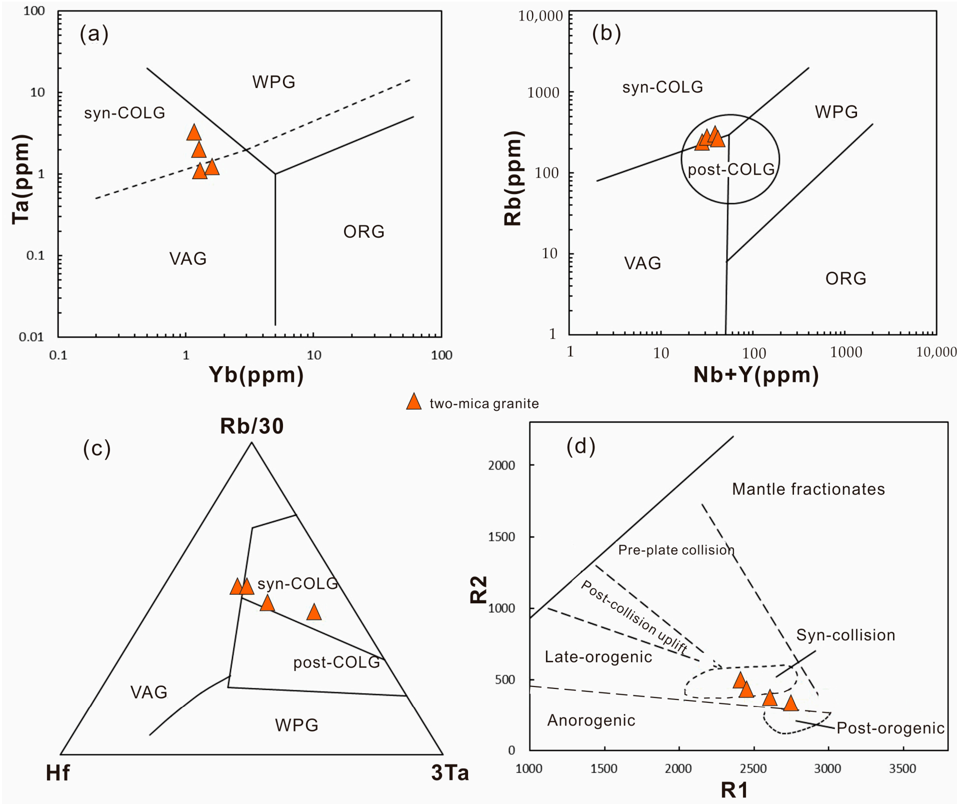

Figure 8. (**a**,**b**) Ta-Yb and Rb-(Nb + Y) discriminant diagrams [57]; (**c**) Rb-Hf-Ta triangular plot discriminant diagrams [58]; (**d**) R2 vs. R1 discriminant diagrams [59]. syn-COLG: syn-collision granites; VAG: volcanic arc granites; WPG: within-plate granites; ORG: ocean ridge granites; post-COLG: post-collision granites. R1 = 4Si − 11(Na + K) − 2(Fe + Ti); R2 = 6Ca + 2Mg + Al. Data from Tables 1 and 2.

The zircon U-Pb dating of the Ke'eryin two-mica granite shows that its crystallization age is 219.2 ± 2.3 Ma [31], and the zircon U-Pb age of the adjacent Jiajika two-mica granite is 223 ± 1 Ma [60], both of which were formed in the Late Triassic–Early Jurassic period. Based on the geochemical characteristics of the whole rock, the tectonic environment and process of granite formation in the mining area can be inferred as follows: with the closing of the Southern Paleo-Tethys Ocean Basin at the end of the Triassic period, continental collision occurred in the Yangtze block, North China Block and Qiangtang block, resulting in crustal thickening and the partial melting of crust-source materials to form granite in the region. The bidirectional contraction of the Songpan–Garze orogenic belt was caused by the collision, which resulted in large-scale slip nappe structures, accompanied by strong magmatic and metamorphic activities in the area, which formed several important compound dome structures in the eastern part of the orogenic belt [35,61], providing a good tectonic environment for the mineralization of pegmatite.

6.2. Indications of Mica for the Evolution of Pegmatite

The formation of granite pegmatite is a highly evolved magmatic–hydrothermal process [62]. The initial magma-forming pegmatites, due to the crystallization differentiation, lead to the enrichment and saturation of volatiles in the residual melt [63–65], while the magmatic fluid phase exsolution occurs and forms an independent water-bearing fluid phase, thus entering the magmatic–hydrothermal transition stage [66]. As the melt phase finally crystallized completely, the system entered the hydrothermal stage. During the evolution of pegmatite magma, the changes in the K/Rb ratio, Nb/Ta ratio, and Li, Rb and Cs contents of mica can indicate the trend and degree of magmatic–hydrothermal differentiation and evolution. With the gradual increase in magmatic differentiation and evolution, the contents of volatile elements Li and incompatible elements Rb and Cs also increase, while the ratios of K/Rb and Nb/Ta decrease [67–73]. In highly evolved magmatic systems, the K/Rb ratio is usually reduced to less than 50 [74,75].

In this study, the K/Rb ratio of MAP to ASP mica varies from 9.76 to 42.02, which generally exhibits the characteristics of high magmatic evolution. The mica composition in Lijiagou pegmatite displays evolutionary characteristics (Figure 9). The contents of Li, Rb, Cs, and F in mica gradually increase, and the K/Rb ratio gradually decreases (Figure 9a–c,f), indicating that the degree of magmatic evolution is increasing, and the type of mica also shows the evolution characteristics of muscovite to Li-bearing mica. The contents of Li, Rb, and Cs of Li-bearing mica in ASP reached the highest value, and the content of F also increased from 0.41%–5.86% to 8.94%–10.87%, indicating that the magmatic evolution reached a very high degree at this stage. In this stage, Li-bearing mica mainly appeared as the secondary form on the edges of primary muscovite, with a metasomatic structure, which may be attributed to late Li-rich fluid metasomatic muscovite, and the enrichment of Li and F combined with changes in mica types, indicating the hydrothermal environment [76]. In general, a Li-F rich environment is extremely favorable to the formation of lepidolite, while Li-bearing mica only appears as a secondary form at the edge of the primary muscovite, which may be due to the relatively low F concentration in the pegmatite system [77]. In Figure 9g–i, there is a negative correlation between Nb/Ta and the Li, Rb, and Cs contents of mica. During the evolution process from magmatic to hydrothermal, the generation of the fluid phase also promotes the mineralization of Nb. In the muscovite of MP and MAP, the content of Nb increases slightly, indicating that Nb is gradually enriched in the melt with evolution. However, in the mica of AP and ASP, the content of Nb gradually decreases, indicating that Nb begins to precipitate to form columbite after entering the magmatic–hydrothermal stage and resulting in the gradual loss of Nb (Figure 9d). The variation range of Ta content in mica is small (Figure 9e), which may be because Ta cannot easily replace Al, Fe, and Mg in micas as Nb [78–80]. In addition, the characteristics of fluid inclusions in ASP pegmatites reveal the fluid characteristics of pegmatite magma in the magmatic–hydrothermal transition stage. In the magmatic–hydrothermal transition stage, the fluid properties of the system are volatile-rich silicate fluids. With the decrease in temperature and pressure, the phenomenon of symbiosis between low-salinity, high-density crystal-rich inclusions and high-salinity, low-density CO_2-H_2O inclusions appears, indicating that fluid immiscibility occurs in the system, which is also a critical mechanism of Li enrichment and precipitation in the Lijiagou deposit [19,29]. ASP underwent a magmatic–hydrothermal transformation and post-crystallization hydrothermal process during its formation and evolution, and the high enrichment of Li also occurred in the magmatic–hydrothermal transition stage [30].

Therefore, the Lijiagou barren pegmatite (MP-MAP) transformed into ore-bearing pegmatite (ASP) through a magmatic–hydrothermal evolution process, which resulted in a gradual increase in the degree of evolution. The significant enrichment of rare metals, such as Li, Rb, and Cs, primarily occurred during the magmatic–hydrothermal transition stage.

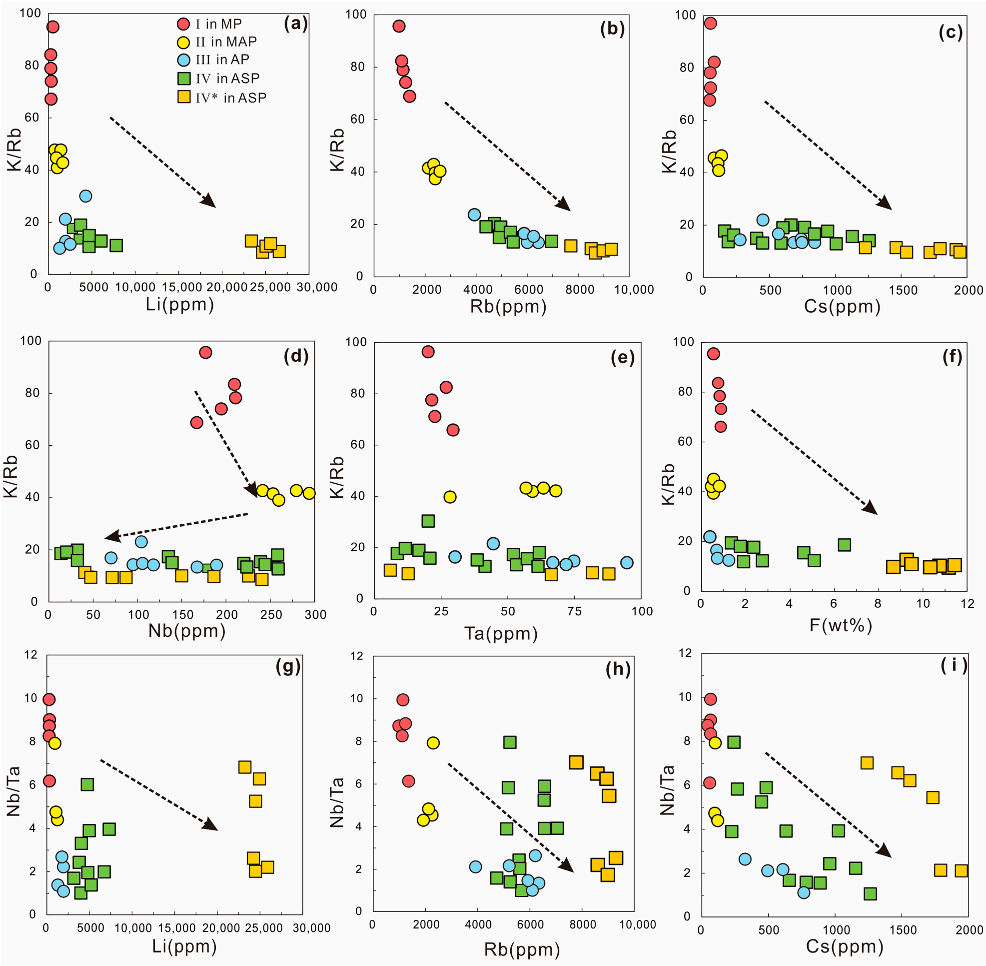

Figure 9. Plots of K/Rb vs. Li (**a**), K/Rb vs. Rb (**b**), K/Rb vs. Cs (**c**), K/Rb vs. Nb (**d**), K/Rb vs. Ta (**e**), K/Rb vs. F (**f**), Nb/Ta vs. Li (**g**), Nb/Ta vs. Rb (**h**) and Nb/Ta vs. Cs (**i**) in micas of different zones from Lijiagou pegmatite. I: muscovite in microcline pegmatite; II: muscovite in microcline albite pegmatite; III: muscovite in albite pegmatite; IV: Li-bearing mica (low Li content) in albite spodumene pegmatite; IV *: Li-bearing mica (high Li content) in albite spodumene pegmatite. MP—microcline pegmatite; MAP—microcline albite pegmatite; AP—albite pegmatite; ASP—albite spodumene pegmatite.

7. Conclusions

(1) The two-mica granite was mainly formed during the transition period from syn-collision to post-collision. After the end of the continental collision, the crust was squeezed and thickened into the post-collision extensional transition tectonic environment, The favorable tectonic environment contributed to the formation of the Lijiagou pegmatite-type spodumene deposit.

(2) From MP to ASP, the micas in Lijiagou pegmatite exhibit an evolutionary trend from muscovite to Li-bearing mica. From MP to AP, muscovite is the main type. Starting from ASP, the type of mica begins to change. The Li-bearing mica appears in the secondary form, at the edge of the primary muscovite, and has a metasomatic structure. This may be the result of the subsequent Li-rich fluid metasomatism of muscovite. The mineral chemical characteristics of mica indicate that the Lijiagou pegmatite has a high degree of differentiation and evolution, and the degree of evolution gradually increases from MP to ASP.

(3) Lijiagou pegmatite experienced magmatic–hydrothermal evolution. From MP to ASP, there is a negative correlation between Nb/Ta, K/Rb and the Li, Rb and Cs contents of mica, while the contents of Li, Rb, Cs and F in Li-bearing mica of ASP increased sharply.

Combined with the change in mica type, it is considered that ASP formed during the transition from magmatic to hydrothermal and was a fluid-rich environment, and Li, Rb, and Cs mainly began to enrich during the magmatic–hydrothermal transition.

Author Contributions: Conceptualization, X.C. and C.C.; methodology, X.C.; validation, X.L. and Y.Y.; investigation, X.C. and X.L.; resources, Y.C.; data curation, X.C., X.L. and Y.G.; writing—original draft preparation, X.C.; writing—review and editing, X.C. and C.C.; supervision, C.C.; project administration, C.C.; funding acquisition, C.C. All authors have read and agreed to the published version of the manuscript.

Funding: Sichuan Energy Investment Lithium Technology Co. Ltd. horizontal research project: Research on process mineralogy of spodumene ore, a key technology for development and comprehensive utilization of spodumene ore in western Sichuan, grant number AHG043.

Data Availability Statement: Data supporting the findings of this study will be made available from the corresponding author, upon reasonable request.

Acknowledgments: We would like to thank Fei Guangchun from College of Earth Science, Chengdu University of Technology for guidance and advice. We also thank to Huang Qiaoyuan from Chongqing Survey Institute and Yu Xiao from Petroleum Engineering Technology Research Institute of Sinopec Jianghan Oilfield Company for assistance in field work.

Conflicts of Interest: The authors declare no conflicts of interest.

References

1. Wang, Q.S.; Yuan, Q.H. The global supply situation of lithium ore and suggestions on resources security in China. *China Min. Mag.* **2019**, *28*, 1–6. (In Chinese with English Abstract)
2. Wen, H.J.; Luo, C.G.; Du, S.J.; Yu, W.X.; Gu, H.N.; Ling, K.Y.; Cui, Y.; Li, Y.; Yang, J.H. Carbonate-hosted clay-type lithium deposit and its prospecting significance. *Chin. Sci. Bull.* **2020**, *65*, 53–59. (In Chinese with English Abstract) [CrossRef]
3. Wang, D.H. Study on critical mineral resources: Significance of research, determination of types, attributes of resources, progress of prospecting, problems of utilization, and direction of exploitation. *Acta Geol. Sin.* **2019**, *93*, 1189–1209. (In Chinese with English Abstract)
4. Chakhmouradian, A.R.; Smith, M.P.; Kynicky, J. From "strategic" tungsten to "green" neodymium: A century of critical metals at a glance. *Ore Geol. Rev.* **2015**, *64*, 455–458. [CrossRef]
5. Shearer, C.K.; Papike, J.J.; Jolliff, B.L. Petrogenetic links among granites and pegmatites in the Harney Peak rare element granite-pegmatite system, Black Hills, South Dakota. *Can. Mineral.* **1992**, *30*, 785–809.
6. London, D.; Kontak, D.J. Granitic pegmatites: Scientific wonders and economic bonanzas. *Elements* **2012**, *8*, 257–261. [CrossRef]
7. London, D. Ore-forming processes within granitic pegmatites. *Ore Geol. Rev.* **2018**, *101*, 349–383. [CrossRef]
8. Han, L.; Pan, J.Y.; Ni, P.; Chen, H. Cassiterite deposition induced by cooling of a single-phase magmatic fluid: Evidence from SEM-CL and fluid inclusion LA-ICP-MS analysis. *Geochim. Cosmochim. Acta* **2023**, *342*, 108–127. [CrossRef]
9. Ni, P.; Pan, J.Y.; Han, L.; Cui, J.M.; Gao, Y.; Fan, M.S.; Li, W.S.; Chi, Z.; Zhang, K.H.; Cheng, Z.L.; et al. Tungsten and tin deposits in South China: Temporal and spatial distribution, metallogenic models and prospecting directions. *Ore Geol. Rev.* **2023**, *157*, 105453. [CrossRef]
10. Li, W.S.; Ni, P.; Wang, G.G.; Yang, Y.L.; Pan, J.Y.; Wang, X.L.; Chen, L.L.; Fan, M.S. A possible linkage between highly fractionated granitoids and associated W mineralization in the Mesozoic Yaogangxian granitic intrusion, Nanling region, South China. *J. Asian Earth Sci.* **2020**, *193*, 104314. [CrossRef]
11. Liu, X.H.; Chen, X.Y.; He, L.H.; Zhao, Z.W. Study on extraction of lithium from salt lake brine by men brane electrolysis. *Desalination* **2015**, *376*, 35–40. [CrossRef]
12. Zheng, M.P.; Zhang, Y.S.; Liu, X.F.; Qi, W.; Kong, F.J.; Nie, Z.; Jia, Q.X.; Pu, L.Z.; Hou, X.H.; Wang, H.L.; et al. Progress and prospects of salt lake research in China. *Acta Geol. Sin.* **2016**, *90*, 2123–2165. (In Chinese with English Abstract) [CrossRef]
13. Wang, D.H.; Chen, Y.C.; Jiang, B.; Huang, F.; Wang, Y.; Li, H.Q.; Hou, K.J. Preliminary study on the Triassic continental mineralization system in China. *Earth Sci. Front.* **2020**, *27*, 45–59. (In Chinese with English Abstract)
14. Selway, J.B.; Breaks, F.W.; Tindle, A.G. A review of rare-element (Li-Cs-Ta) pegmatite exploration techniques for the Superior Province, Canada, and large worldwide tantalum deposits. *Explor. Min. Geol.* **2005**, *14*, 1–30. [CrossRef]
15. Černý, P. Petrogenesis of granitic pegmatites. In granitic pegmatites in science and industry. *Mineral. Assoc. Can. Short Course* **1982**, *8*, 293–327.
16. Černý, P.; Anderson, A.J.; Tomascak, P.B.; Chapman, R. Geochemical and morphological features of beryl from the Bikita granitic pegmatite, Zimbabwe. *Can. Min.* **2003**, *41*, 1003–1011. [CrossRef]
17. Romer, R.; Pichanvant, M. Rare metal (Sn, W, Ta-Nb, Li) granites and pegmatites. In *Reference Module in Earth Systems and Environmental Sciences*; Elsevier: Amsterdam, The Netherlands, 2020; pp. 840–846.

18. Li, J.K.; Wang, D.H.; Chen, Y.C. The ore-forming mechanism of the Jiajika pegmatite-type rare metal deposit in western Sichuan province: Evidence form isotope dating. *Acta Geol. Sin. Engl. Ed.* **2013**, *87*, 91–101.
19. Fei, G.C.; Menuge, J.F.; Chen, C.S.; Yang, Y.L.; Deng, Y.; Li, Y.G.; Zheng, L. Evolution of pegmatite ore-forming fluid: The Lijiagou spodumene pegmatites in the Songpan-Garze fold belt, southwestern Sichuan province, China. *Ore Geol. Rev.* **2021**, *139*, 104441. [CrossRef]
20. Deng, J.Y.; Li, J.K.; Zhang, D.H.; Chou, I.M.; Yan, Q.G.; Xiong, X. Origin of pegmatitic melts from granitic magmas in the formation of the Jiajika lithium deposit in the eastern Tibetan Plateau. *Asian Earth Sci.* **2022**, *229*, 105147. [CrossRef]
21. Wang, R.C.; Xie, L.; Zhu, Z.Y.; Hu, H. Micas: Important indicators of granite-pegmatite-related rare-metal mineralization. *Acta Petrol. Sin.* **2019**, *35*, 69–75. (In Chinese with English Abstract)
22. Jolliff, B.L.; Papike, J.J.; Shearer, C.K. Fractionation trends in mica and tourmaline as indicators of pegmatite internal evolution: Bob Ingersoll pegmatite, Black Hills, South Dakota. *Geochim. Et Cosmochim. Acta* **1987**, *51*, 519–543. [CrossRef]
23. Roda, E.; Pesquera, A.; Velasco, F. Micas of the muscovite-lepidolite series from the Fregeneda pegmatites (Salamanca, Spain). *Mineral. Petrol.* **1995**, *55*, 145–157. [CrossRef]
24. Lichtervelde, M.V.; Grégoire, M.; Linnen, R.L.; Béziat, D.; Salvi, S. Trace element geochemistry by laser ablation ICP-MS of micas associated with Ta mineralization in the Tanco pegmatite, Manitoba, Canada. *Contrib. Mineral. Petrol.* **2008**, *155*, 791–806. [CrossRef]
25. Anderson, M.; Lentz, D.; McFarlane, C.; Falck, H. A geological, geochemical and textural study of an LCT pegmatite: Implications for the magmatic versus metasomatic origin of Nb-Ta mineralization in the Moose II pegmatite, NWT, Canada. *J. Geosci.* **2013**, *58*, 299–320. [CrossRef]
26. Kaeter, D.; Barros, R.; Menuge, J.F.; Chew, D.M. The magmatic–hydrothermal transition in rare-element pegmatites from Southeast Ireland: LA-ICP-MS chemical mapping of muscovite and columbite-tantalite. *Geochim. Cosmochim. Acta* **2018**, *240*, 98–130. [CrossRef]
27. Fei, G.C.; Li, B.; Yang, J.; Chen, X.; Luo, W.; Li, Y.; Tang, W.; Gu, C.; Zhong, W.; Yang, G. Geology, Fluid Inclusion Characteristics and H-O-C Isotopes of Large Lijiagou pegmatite spodumene deposit in Songpan-Garze fold belt, Eastern Tibet: Implications for ore Genesis. *Resour. Geol.* **2018**, *68*, 37–50. [CrossRef]
28. Luo, W.; Yang, B.; Gu, C.H.; Li, J.; Pang, L.W. The Geological Characteristics and ore indicators of Lijiagou Super-large Spodumene Deposit in Jinchuan County, Western Sichuan. *Sichuan Nonferrous Met.* **2021**, *2*, 16–18+21. (In Chinese with English Abstract)
29. Deng, Y.; Fei, G.C.; Li, J.; Tang, W.C.; Zhong, W.; Yang, G.B. Study of C-H-O isotopes and geochronology of the Lijiagou pegmatite spodumene deposit in Sichuan Province. *J. Mineral. Petrol.* **2018**, *38*, 40–47. (In Chinese with English Abstract)
30. Yuan, Y.B.; Chen, B.; Shang, L.B.; Sendula, E.; Chou, M.I. Lithium enrichment of the magmatic-hydrothermal fluid in albite-spodumene pegmatite from Lijiagou, Eastern Tibetan Plateau: Evidence from fluid inclusions. *Ore Geol. Rev.* **2023**, *162*, 105685. [CrossRef]
31. Fei, G.C.; Menuge, J.F.; Li, Y.Q.; Yang, J.Y.; Deng, Y.; Chen, C.S.; Yang, Y.F.; Yang, Z.; Qin, L.Y.; Zheng, L.; et al. Petrogenesis of the Lijiagou spodumene pegmatites in Songpan-garze fold belt, west Sichuan, China: Evidence from geochemistry, zircon, cassiterite and coltan U-Pb geochronology and Hf isotopic compositions. *Lithos* **2020**, *364*, 105555. [CrossRef]
32. Xu, J.B.; Fei, G.C.; Qin, L.Y.; Yang, J.Y.; Zheng, L.; Tang, W.C. LA-MC-ICP-MS U-Pb dating of cassiterite from the Lijiagou pegmatite-type rare-metal deposit in the Ke'eryin orefield, Sichuan province and its geological implication. *Geol. Explor.* **2020**, *56*, 346–358. (In Chinese with English Abstract)
33. Weislogel, A.L.; Graham, S.A.; Chang, E.Z.; Wooden, J.L.; Gehrels, G.E. Detrital zircon provenance from three turbidite depocenters of the Middle-Upper Triassic Songpan-Ganzi complex, central China: Record of collisional tectonics, erosional exhumation, and sediment production. *Geol. Soc. Am. Bull.* **2010**, *122*, 2041–2062. [CrossRef]
34. Zhao, Z.B.; Du, J.X.; Liang, F.H. Structure and metamorphism of Markam gneiss dome from the eastern Tibetan plateau and its implications for crustal thickening, metamorphism, and exhumation. *Geochem. Geophys. Geosyst.* **2019**, *20*, 24–45. [CrossRef]
35. De Sigoyer, J.; Vanderhaeghe, O.; Duchêne, S.; Billerot, A. Generation and emplacement of Triassic granitoids within the Songpan Ganze accretionary-orogenic wedge in a context of slab retreat accommodated by tear faulting, Eastern Tibetan Plateau, China. *Asian Earth Sci.* **2014**, *88*, 192–216. [CrossRef]
36. Xu, Z.Q.; Fu, X.F.; Wang, R.C.; Li, G.W.; Zheng, Y.L.; Zhao, Z.B.; Lian, D.Y. Generation of lithium-bearing pegmatite deposits within the Songpan-Ganze orogenic belt. East Tibet. *Lithos* **2020**, *354–355*, 105281. [CrossRef]
37. Deschamps, F.; Duchêne, S.; Sigoyer, J.; Bosse, V.; Benoit, M.; Vanderhaeghe, O. Coeval mantle-derived and crust-derived magmas forming two neighbouring plutons in the Songpan Garze accretionary orogenic wedge (SW China). *J. Petrol.* **2018**, *58*, 2221–2256. [CrossRef]
38. Li, J.K. Mineralizing Mechanism and Continental Geodynamics of Typical Pegmatite Deposits in Western Sichuan, China. Ph.D. Thesis, China University of Geosciences, Beijing, China, 2006; 61p.
39. Gu, C.H.; Huang, W.J.; Zhou, J.R.; Li, J.; Luo, W.; Jiang, J. *The Reserve Estimation and Detailed Investigation Report of the Dangba Spodumene Pegmatite in Markam Country, Sichuan*; Unpublished Reports; Geochemistry Exploration Team of the Sichuan Bureau of Geology and Mineral Resources Exploration: Deyang, China, 2013; pp. 41–44. (In Chinese)
40. Li, J.K.; Wang, D.H.; Fu, X.F. $^{40}Ar/^{39}Ar$ ages of the Ke'eryin pegmatite type rare metal deposit, Western Sichuan, and its tectonic significances. *Acta Geol. Sin.* **2006**, *80*, 843–848. (In Chinese with English Abstract)

41. Fei, G.C.; Li, T.R.; Menuge, J.F.; Hui, Z.Q.; Yuan, Y.W.; Zhu, H.P.; Tan, H.; Cai, Y.H.; Tang, W.C.; Yang, G.B.; et al. Petrogenesis of aplites in the Ke'eryin rare metal ore field in the Songpan-Garze Fold Belt, Eastern Tibet: Evidence from mineralogy, geochemistry, geochronology and Hf-Nd isotopes. *Lithos* **2023**, *438*, 107017. [CrossRef]
42. Che, X.D.; Wu, F.Y.; Wang, R.C.; Gerdes, A.; Ji, W.Q.; Zhao, Z.H.; Yang, J.H.; Zhu, Z.Y. In situ U-Pb isotopic dating of columbite–tantalite by LA–ICP–MS. *Ore Geol. Rev.* **2015**, *665*, 978–989. [CrossRef]
43. Yan, Q.H.; Qiu, Z.W.; Wang, H.; Wang, M.; Wei, X.P.; Li, P.; Zhang, R.Q.; Li, C.Y.; Liu, J.P. Age of the Dahongliutan rare metal pegmatite deposit, West Kunlun, Xinjiang (NW China): Constraints from LA–ICP–MS U–Pb dating of columbite-(Fe) and cassiterite. *Ore Geol. Rev.* **2018**, *100*, 561–573. [CrossRef]
44. Zhang, R.Q.; Lehmann, B.; Seltmann, R.; Sun, W.D.; Li, C.Y. Cassiterite U–Pb geochronology constrains magmatic-hydrothermal evolution in complex evolved granite systems: The classic Erzgebirge tin province (Saxony and Bohemia). *Geology* **2017**, *45*, 1095–1098. [CrossRef]
45. Tan, X.J.; Wang, Z.M. General high-pressure closed acidic decomposition method of rock samples for trace element determination using-inductively-coupled-plasma-mass-spectrometry. *J. Anal. Chem.* **2020**, *75*, 1295–1303.
46. Li, H.; Gan, J.; He, Z.W.; Gan, Y.; Wang, B.; Li, Y.; Jiang, W. Petrogenesis and Geodynamic Significance of the Early Triassic Nanpo Adakitic Pluton of the Luang Prabang-Loei Tectonic Belt (Northwestern Laos) in the East Tethys Domain: Constraints from Zircon U-Pb-Hf Isotope Analyses and Whole-Rock Geochemistry. *Minerals* **2023**, *13*, 821. [CrossRef]
47. Liu, Y.S.; Hu, Z.C.; Gao, S.; Günther, D.; Xu, J.; Gao, C.G.; Chen, H.H. In situ analysis of major and trace elements of anhydrous minerals by LA-ICP-MS without applying an internal standard. *Chem. Geol.* **2008**, *257*, 34–43. [CrossRef]
48. Li, J.K.; Zhang, D.H.; Wang, D.H.; Zhang, W.H. Liquid Immiscibility of Fluorine-rich Granite Magma and Its Diagenesis and Metallogeny. *Geol. Rev.* **2008**, *54*, 175–183, (In Chinese with English Abstract).
49. Webster, J.D.; Thomas, R.; Rhede, D.; Förster, H.J.; Seltmann, R. Melt inclusions in quartz from an evolved peraluminous pegmatite: Geochemical evidence for strong tin enrichment in fluorine-rich and phosphorus-rich residual liquids. *Geochim. Cosmochim. Acta* **1997**, *61*, 2589–2604. [CrossRef]
50. Middlemost, E.A.K. Naming materials in the magma/igneous rock system. *Earth-Sci. Rev.* **1994**, *37*, 215–224. [CrossRef]
51. Maniar, P.D.; Piccoli, P.M. Tectonic discrimination of granitoids. *Geol. Soc. Am. Bull.* **1989**, *101*, 635–643. [CrossRef]
52. Peccerillo, A.; Taylor, S.R. Geochemistry of eocene calc-alkaline volcanic rocks from the Kastamonu area, Northern Turkey. *Contrib. Mineral. Petr.* **1976**, *58*, 63–81. [CrossRef]
53. Wright, J.B. A simple alkalinity ratio and its application to questions of non-orogenic granite genesis. *Geol. Mag.* **1969**, *106*, 370–384. [CrossRef]
54. Sun, S.S.; McDonough, W.F. Chemical and isotopic systematics of oceanic basalts: Implications for mantle composition and processes. *Geol. Soc. Lond. Spec. Publ.* **1989**, *42*, 313–345. [CrossRef]
55. Fan, G.; Li, G.W.; Shen, G.F.; Xu, J.S.; Dai, J. Luanshiweiite: A New Member of Lepidolite Series. *Acta Mieralogica Sin.* **2013**, *33*, 713–721. (In Chinese with English Abstract)
56. Qu, K.; Sima, X.Z.; Li, G.W.; Fan, G.; Shen, G.F.; Liu, X.; Xiao, Z.B.; Guo, H.; Qiu, L.F.; Wang, Y.J. Fluorluanshiweiite, $KLiAl_{1.5}\square_{0.5}(Si_{3.5}Al_{0.5})O_{10}F_2$, a New Mineral of the Mica Group from the Nanyangshan LCT Pegmatite Deposit, North Qinling Orogen, China. *Minerals* **2020**, *10*, 93. [CrossRef]
57. Pearce, J.A.; Harris, N.B.W.; Tindle, A.G. Trace element discrimination diagrams for the tectonic interpretation of granitic rocks. *J. Petrol.* **1984**, *25*, 956–983. [CrossRef]
58. Harris, N.B.W.; Pearce, J.A.; Tindle, A.G. Geochemical characteristics of collision-zone magmatism. *Geol. Soc. Lond. Spec. Publ* **1986**, *19*, 67–81. [CrossRef]
59. Batchelor, R.A.; Bowden, P. Petrogenetic Interpretation of Granitoid Rock Series Using Multicationic Parameters. *Chem. Geol.* **1985**, *48*, 43–55. [CrossRef]
60. Hao, X.F.; Fu, X.F.; Liang, B.; Yuan, L.P.; Pan, M.; Tang, Y. Formation ages of granite and X03 pegmatite vein in Jiajika, western Sichuan, and their geological significance. *Miner. Depos.* **2015**, *34*, 1199–1208. (In Chinese with English Abstract)
61. Xu, Z.Q.; Hou, L.W.; Wang, Z.X.; Fu, X.F.; Huang, M.H. *Orogenic Process of the Songpan-Ganzi Orogenic Belt*; Geological Publishing House: Beijing, China, 1992; pp. 1–202. (In Chinese)
62. Černý, P.; Meintzer, R.E.; Anderson, A.J. Extreme fractionation in rare-element granitic pegmatites: Selected examples of data of mechanisms. *Can. Mineral.* **1985**, *23*, 381–421.
63. London, D. Magmatic-hydrothermal transition in the Tanco rare-metal pegmatite: Evidence from fluid inclusions and phase-equilibrium experiments. *Am. Mineral.* **1986**, *71*, 376–395.
64. London, D. Internal differentiation of rare-element pegmatites: Effects of boron, phosphorus, and fluorine. *Geochim. Cosmochim. Acta* **1987**, *51*, 403–420. [CrossRef]
65. Thomas, R.; Webster, J.D.; Heinrich, W. Melt inclusions in pegmatite quartz: Complete miscibility between silicate melts and hydrous fluids at low pressure. *Contrib. Mineral. Petrol.* **2000**, *139*, 394–401. [CrossRef]
66. Burnham, C.W.; Ohmoto, H. Late stage processes of felsic magmatism. *Min. Geol. Spec. Issue* **1980**, *8*, 1–11.
67. Wise, M.A. Trace element chemistry of lithium-rich micasfrom rare-element granitic pegmatites. *Mineral. Petrol.* **1995**, *55*, 203–221. [CrossRef]
68. Roda-Robles, E.; Pesquera, A.; Gil-Crespo, P.; Torres-Ruiz, J. From granite to highly evolved pegmatite: A case study of thePinilla de Fermoselle granite-pegmatite system (Zamora, Spain). *Lithos* **2012**, *153*, 192–207. [CrossRef]

69. Roda-Robles, E.; Keller, P.; Pesquera, A. Micas of the muscovite-lepidolite series from Karibib pegmatites, Namibia. *Mineral. Mag.* **2007**, *71*, 41–62. [CrossRef]
70. Garate-Olave, I.; Müller, A.; Roda-Robles, E. Extreme fractionation in a granite–pegmatite system documented by quartz chemistry: The case study of Tres Arroyos (Central Iberian Zone, Spain). *Lithos* **2017**, *286–287*, 162–174. [CrossRef]
71. Icenhower, J.; London, D. An experimental study of element partitioning among biotite, muscovite, and coexisting peraluminous silicic melt at 200 MPa (H_2O). *Am. Miner.* **1995**, *80*, 1229–1251. [CrossRef]
72. Hulsbosch, N.; Hertogen, J.; Dewaele, S.; André, L.; Muchez, P. Alkali metal and rare earth element evolution of rock-forming minerals from the Gatumba area pegmatites (Rwanda): Quantitative assessment of crystal-melt fractionation in the regional zonation of pegmatite groups. *Geochim. Cosmochim. Acta* **2014**, *132*, 349–374. [CrossRef]
73. Ballouard, C.; Poujol, M.; Boulvais, P.; Branquet, Y.; Tartèse, R.; Vigneresse, J.L. Nb-Ta fractionation in peraluminous granites: A marker of the magmatic-hydrothermal transition. *Geology* **2016**, *44*, 231–234. [CrossRef]
74. Irber, W. The lanthanide tetrad effect and its correlation with K/Rb, Eu/Eu, Sr/Eu, Y/Ho, and Zr/Hf of evolving peraluminous granite suites. *Geochim. Cosmochim. Acta* **1999**, *63*, 489–508. [CrossRef]
75. Shaw, D.M. A review of K-Rb fractionation trends by covariance analysis. *Geochim. Cosmochim. Acta* **1968**, *32*, 573–601. [CrossRef]
76. Wang, Z.; Chen, Z.Y.; Li, J.K.; Li, P.; Xiong, X.; Yang, H.; Zhou, F.C. Indication of mica minerals for magmatic-hydrothermal evolution of Renli rare metal pegmatite deposit. *Miner. Depos.* **2019**, *38*, 1039–1052. (In Chinese with English Abstract)
77. Yin, R.; Huang, X.L.; Xu, Y.G.; Wang, R.C.; Wang, H.; Yuan, C.; Ma, Q.; Sun, X.M.; Chen, L.L. Mineralogical constraints on the magmatic-hydrothermal evolution of rare-elements deposits in the Bailongshan granitic pegmatites, Xinjiang, NW China. *Lithos* **2020**, *352–353*, 105208. [CrossRef]
78. Mu, S.T.; Shao, Y.J.; Song, Z.Y.; Zhou, H.X.; Liu, Q.Q.; Xiong, Y.Q. Geochemical characteristics and indication of mica in Renli—Chuanziyuan pegmatite type rare metal deposit in Hunan Province. *J. Cent. South Univ.* **2021**, *52*, 2973–2989.
79. Linnen, R.L.; Keppler, H. Columbite solubility in granitic melts: Consequences for the enrichment and fractionation of Nb and Ta in the Earth's crust. *Contrib. Mineral. Pet.* **1997**, *128*, 213–227. [CrossRef]
80. López-moro, F.J.; García, F.; Llorens, T.; Luis, J.; Contreras, S.; Fernández, A.; Candelas, M.; Benito, M. Ta and Sn concentration by muscovite fractionation and degassing in a lens-like granite body: The case study of the Penouta rare-metal albite granite (NW Spain). *Ore Geol. Rev.* **2017**, *82*, 10–30. [CrossRef]